博 士 論 文

Preparation and Properties of Fluorescent Orthodontic Adhesives Containing $Y_2O_3:Eu^{3+}$ Particles

($Y_2O_3:Eu^{3+}$微粒子含有矯正歯科用蛍光ボンディング剤の製造と特性)

平成 25 年 3 月申請

北海道大学

大学院歯学研究科口腔医学専攻

半 場 悠 介

Synopsis

Orthodontic adhesives are typically colorless and transparent for aesthetic purposes. The utilization of fluorescence is one of the most effective solutions to make the adhesives visible for safe and complete removal after orthodontic treatments. Eu^{3+} ions were doped into yttrium oxides (Y_2O_3) using a homogeneous precipitation method. The crystals synthesized in this study exhibited submicron sizes and a very narrow size distribution. The X-ray diffraction (XRD) patterns agreed well with the known diffraction patterns of Y_2O_3, and indicated an absence of any other crystalline substances. Therefore, it was determined that the crystals synthesized in this study were in fact Y_2O_3:Eu^{3+}. The spectra of the poly(methyl methacrylate) (PMMA) adhesives containing Y_2O_3:Eu^{3+} particles exhibited characteristic excitation and emission peaks corresponding to the 4f-4f transitions of Eu^{3+}, despite the photoluminescence intensity being relatively low. The yielding loads of the Y_2O_3:Eu^{3+} particles contained in the PMMA specimens did not deteriorate by a significant amount. We conclude that it is feasible to add the Eu^{3+}-doped Y_2O_3 crystalline particles into orthodontic adhesives.

Key words: *fluorescence, lanthanide, europium, yttria oxide, orthodontic adhesive*

Introduction

After orthodontic treatment using multibracket appliances (Fig. 1), the removal of any residual resin-based adhesives through the use of rotary dental instruments is necessary. Since orthodontic adhesives are either transparent or similar to the color of teeth, the enamel surfaces can easily be damaged during the removal process [1-5]. Figure 2 displays a scanning electron microscopy (SEM) image as an example of a damaged enamel surface (damaged areas indicated by arrows) after the removal of an orthodontic adhesive. Utilizing fluorescent orthodontic adhesives may be a possible solution for this problem.

Trivalent lanthanide ions are well-known and widely used fluorescent substances [6,7]. The Eu^{3+} ion which is one of the most popular lanthanides, is useful for the development of a fluorescent orthodontic adhesive because Eu^{3+} emits highly monochromatic red light when it is excited with near-ultraviolet (UV) light [8,9].

Yttrium oxide (Y_2O_3) is a well-known host material for enhancing the photoluminescence (PL) intensity of luminescent centers such as lanthanide ions, and possesses excellent physical properties, a high chemical durability, and a high biocompatibility [10-14]. Sharma et al.

reported that the emission intensity could be increased by reducing the average size of the Y_2O_3:Eu^{3+} particles from 6 μm to 0.2 μm [15]. Goldburt et al. reported that the nonradiative transition decreased as the particle size decreased [16]. Therefore, we selected fine-grain Y_2O_3 particles containing Eu^{3+} (Y_2O_3:Eu^{3+}) as a possible phosphor candidate for fluorescent orthodontic adhesives.

In this study, the morphology and the fluorescence properties of Y_2O_3:Eu^{3+} particles were investigated. Furthermore, both the fluorescence and mechanical properties of poly(methyl methacrylate)/methyl methacrylate (PMMA/MMA) resin specimens containing Y_2O_3:Eu^{3+} particles were examined.

Materials and methods

1. Synthesis and microstructure of Y_2O_3:Eu^{3+} powder

Yttrium (III) nitrate hexahydrate [$Y(NO_3)_3$•$6H_2O$, purity of 99.99%; Kanto Chemical, Co., Inc., Tokyo, Japan] and europium nitrate hexahydrate [$Eu(NO_3)_3$•$6H_2O$, purity of 99.95%; Kanto Chemical, Co., Inc., Tokyo, Japan] and urea (Kanto Chemical, Co., Inc., Tokyo, Japan) were purchased and used without further purification. $Y(NO_3)_3$•$6H_2O$ (12 mmol) and $Eu(NO_3)_3$•$6H_2O$ (less than 0.3 mmol) were dissolved in 100 mL of deionized water. After CH_4N_2O (1.2 mol/200 mL) was added to the aqueous solution, stirring for 90 min was carried out at 97-100°C [8], and a white precipitate of basic carbonate of yttrium and europium was subsequently obtained. After the precipitate was centrifuged and washed with deionized water, it was fired at 1,105°C in air for 1 h. The obtained powder was then ground in a mortar and pestle to obtain a narrow particle size distribution.

The microstructure of the particles was examined using SEM (S-4000, Hitachi, Tokyo, Japan) and transmission electron microscopy (TEM) (H-800, Tokyo, Japan) operating at accelerating voltages of 10 kV and 300 kV, respectively. X-ray diffraction (XRD) analyses were carried out using a diffractometer (Multi Flex/HS, Rigaku, Tokyo, Japan) at a scanning rate of 1°/min with Cu $K\alpha_1$ radiation (λ = 0.15405 nm) at 40 kV / 20 mA. Additionally, energy dispersive X-ray spectrometry (EDS) analysis was performed using an SEM (S-2380N, Hitachi, Tokyo, Japan) equipped with an EDS spectroscope (Genesis CDU, AMETEK EDAX, Tokyo, Japan) operated at an accelerating voltage of 10 kV.

2. Fabrication and properties of the PMMA resin containing the synthesized particles

The PMMA/MMA resin used in this study contains tertiary amines as polymerization accelerators within the MMA liquid and benzoyl peroxide as a polymerization initiator within the PMMA powder. A series of partially substituted PMMA powders containing 2% or 4% of the particles were prepared prior to polymerization. Cylindrical specimens (3 mm in diameter and 4 mm in height) in which the particles were dispersed in PMMA/MMA were then polymerized at room temperature. Additionally, additive-free PMMA specimens of the same shape and dimensions were also fabricated in the same manner. All specimens underwent heating at 100°C for 1 h in order to release the residual monomers.

The fluorescent properties of both the particles and the fabricated PMMA specimens containing the particles were observed macroscopically using a light emitting diode (LED) with a central wavelength of 375 nm as the source of near-UV light irradiation. Furthermore, the fluorescence spectra of the particles-containing PMMA specimens were measured using a fluorescence spectrophotometer (F-4010, Hitachi, Tokyo, Japan) under the following conditions: a spectral band pass of 2.5 nm and a wavelength scanning speed of 60 nm/min.

Compression tests were performed using a universal testing machine (Model 4202, Instron Corp, Canton, MA) with a 1.0 mm/min crosshead speed, and the yielding stress was subsequently measured. Eighteen specimens for each particle content percentage (0%, 2%, or 4%) were examined. These results were then statistically analyzed using the Mann-Whitney U test at a level of significance of $\alpha = 0.01$.

Results

1. Microstructures of the synthesized particles

An SEM image and a TEM image of the particles are displayed in Fig. 3 and Fig. 4, respectively. The particles exhibited a strong tendency to agglomerate, as shown in Fig. 3. The size of the crystals varied by a small amount, and was approximately 100 nm in diameter (Fig. 3, Fig. 4).

Figure 5 displays the XRD patterns of the particles. Additionally, vertical bars were incorporated in the image to indicate the standard peak positions and heights of Y_2O_3. This result revealed that the XRD pattern of the particles was in accordance with that of Y_2O_3. The EDS spectrum (Fig.6) confirms the presence of Y and Eu within the particles.

2. Observations and measurements of the fluorescence originating in the particles

Figure 7 and 8 display the macroscopic features of the particles and the PMMA specimens that

contained particles, respectively. The particles exhibited a clear red emission upon irradiating with near-UV light at 375 nm (Fig. 7b), despite appearing white in color under natural light (Fig. 7a). As shown in Fig. 8a, the specimens containing the particles were an opaque white color. The degree of opaqueness increased as the amount of particles increased. The fluorescence of the PMMA/MMA specimens upon irradiation with near-UV light exhibited a pale red emission, regardless of the amount of particles contained within (Fig. 8b). The emission intensity slightly increased as the amount of particles increased as observed macroscopically. However, the PMMA/MMA specimens exhibited lower fluorescence intensity than the particles.

Figure 9a displays the excitation spectrum of the PMMA/MMA specimens by monitoring the emission at λ = 614 nm. Peaks at 396, 416, 466, and 534 nm were then observed in the excitation spectrum (Fig. 9a). The emission spectrum of the PMMA/MMA samples containing the particles at the excitation of 396 nm is shown in Fig. 9b. Additionally, the transition of energy states responsible for each fluorescence peak are indicated in the Fig.9b. The strongest emission peak was observed at 614 nm.

3. Mechanical properties of the PMMA containing particles

Figure 10 displays the results of the compression tests for both the additive-free PMMA specimens (0% specimen) and the PMMA specimens containing the particles (2% and 4% specimens). The error bars on the bar graph represent the standard deviation of the mean. The inserted figure is an exemplary stress-strain curve of a PMMA specimen containing particles used in this study in order to explain the yielding point of a soft material without compression failure. The stress-strain curves of all specimens obtained in this study exhibited very similar deformation behavior. Therefore, we used the yielding stress to evaluate the mechanical properties of the samples. No statistical significance existed between the yielding stress of the 0% specimen and the 4% specimen. Meanwhile, the yielding stress of the 2% specimen was significantly smaller than that of 0% and 4% specimens ($p < 0.01$).

Discussion

1. Fabrication and morphology of the synthesized particles

In general, orthodontic adhesives are typically colorless for aesthetic purposes. Eu^{3+} was chosen as a luminescent center to develop a fluorescent orthodontic adhesive because it exhibits colorless characteristics under natural light. Additionally, even under the conditions of normal

dental practices, the adhesives could be visually distinguished from the enamel surfaces because of the highly monochromatic red luminescence of Eu^{3+}, which also exhibits a large Stokes shift (an intrinsic difference in wavelength between the excitation and emission maxima of a fluorescent substance). The large stokes shift makes the fluorescence light discriminable from the irradiation light easily.

It has been previously reported that phosphor materials must have a small size (< 3 μm), a narrow size distribution, and non-agglomeration in order to produce ideal luminescent characteristics [12,17,18]. A wide variety of methods have been proposed to prepare small metal oxide particles with a narrow size distribution [8-16,18-46]. With respect to the phase of a given materials, these methods can be categorized into three categories: solid-phase methods, liquid-phase methods, and vapor-phase condensation. Solid-phase methods include thermal dissociation [19,20] and mechanical milling [21,22]. Liquid-phase methods utilize homogeneous precipitation [8,9,14,23-29], the co-precipitation method [15], conventional hydrothermal methods [30-35], microwave-assisted hydrothermal treatment [11,13], the sol-gel technique [16,36-39], and the solvothermal refluxing method [10,12,40,41]. Vapor-phase methods include chemical vapor deposition [42], solution combustion [43,44], and spray pyrolysis methods [18,45,46]. Among these methods, it is generally accepted that the homogeneous precipitation method is the most useful for the preparation of fine particles with a relatively narrow size distribution [14,28]. Therefore, we used the homogeneous precipitation method for the Y_2O_3:Eu^{3+} co-precipitation. The synthesized crystals exhibited a submicron size and their size distribution was quite narrow (Fig. 4). The uniform size of the particles could possibly be the result of grinding with a mortar and pestle. If that phenomenon is in fact true, then lattice defects may have occurred in exchange for obtaining the uniform submicron morphology, and those defects may be a factor in decreasing the emission intensity [47].

In addition to effects of the particle size and their uniformity on the PL, the spherical morphology was recognized as an important factor for enhancing the PL intensity. The spherical morphology is ideal for high brightness because of low scattering of light associated with spherical materials [12,17,18,26,34]. The particles obtained in this study likely consist of plural crystals that were sintered during the firing procedure we employed (Fig. 4). In fact, the particles were somewhat cubic instead of spherical in shape. This result is because the higher firing temperature (above 1000°C for Y_2O_3) yields better crystallization, and densification could occur above 1100°C [48]. We selected the firing temperature (1105°C) based on the influence of the firing temperatures on the sizes and luminescence intensities of the Y_2O_3:Eu^{3+} particles

[26,34]. Jing et al. reported that the luminescence of the particles increased as the firing temperatures increased from 800 to 1050°C [26]. They also stated that the relative luminescence reached a plateau when the particle size was above 0.9 μm. Jiang et al. reported that the average particle size exhibited a sharp increase as the firing temperature increased, especially above 1200°C [34]. They also mentioned that further firing resulted in a decrease in the luminescence efficiency as a result of the scattering of light by the surfaces of voids in hard agglomerations. It has been well established that the commercial Y_2O_3:Eu^{3+} phosphors (3–5 μm in size) are fired at temperatures above 1500°C [26,47]. Nevertheless, the luminescence intensity of the commercial phosphors is quite high. For this reason, the luminescence efficiency may be attributed to their single crystalline phase after firing at such high temperatures.

The XRD pattern of the crystalline products agrees well with the known diffraction pattern of Y_2O_3 (Fig. 5). The known peak that characterizes the existence of crystalline europium(III) oxide (Eu_2O_3) should be observed at $2\theta = 28.4°$; however, no peak corresponding to Eu_2O_3 was observed. The slightly larger lattice parameter of Eu_2O_3, when incorporated into the Y_2O_3 lattice, could shift the (222) peak to a lower angle. However, the peak appears not to shift with respect to the typical (222) peak. Therefore, it was determined that the crystals synthesized in this study were in fact Y_2O_3:Eu^{3+}.

2. Macroscopic features and photoluminescence of PMMA containing Y_2O_3:Eu^{3+} particles

The macroscopic appearance of the additive-free PMMA specimen was colorless and transparent. Alternatively, the PMMA specimens containing the Y_2O_3:Eu^{3+} particles became white and opaque. The particles strongly agglomerated, as shown in Fig. 3 and such hard agglomerations are likely to create a high concentration of packing voids [34]. Therefore, an increased scattering cross-section due to both the large agglomerates and the resulting packing voids is believed to be the primary cause of the adhesives becoming opaque when the particles are introduced. The increased scattering cross-section also causes the light from the emission to be difficult to reach the human eye. This phenomenon is most likely responsible for the fluorescence intensity being very weak. Future research into reducing the high degree of agglomeration and improving the dispersing quality of the particles within the polymer matrix is required.

The 15 trivalent lanthanide ions (Ln^{3+}) possess electronic configurations of $[Xe]4f^{0-14}5d^{0-1}6s^2$, which generate a variety of electronic levels. It has been well established that most of the sharp PL peaks are a result of the energy transitions between the states of the $4f^n$ (n

= 0–14) configuration. There were no significant shifts in the emission peaks of Ln^{3+} due to the shielding by the $5s^25p^6$ electrons [49]. However, it is generally accepted that the 4f-4f transitions are intrinsically forbidden. Therefore, not all transitions are permitted since they must obey the selection rules. One of these particular rules is the parity rule, which is required for the electric dipole (ED) transition [7]. This rule provides an explanation why the forbidden 4f-4f transition occurs in Eu^{3+}. The selection rules and transition probabilities between various states strongly depend on a crystal field in which the substitution of Eu^{3+} is taking place [49]. A Eu^{3+} ion, when it is inserted within a Y_2O_3 crystal, can occupy either a low symmetry site (C_2) or a high symmetry site (C_{3i}) [50]. If a Eu^{3+} ion occupies a site exhibiting inversion symmetry (C_{3i}), then the ED transition is forbidden. Meanwhile, if a Eu^{3+} ion occupies a site without inversion symmetry (C_2), then ED transitions such as $^5D_0 \rightarrow {}^7F_2$ or $^5D_0 \rightarrow {}^7F_4$ are allowed. The clear emission peaks resulting from excitation at 396 nm light (as shown in Fig. 9b) are caused by the $^5D_0 \rightarrow {}^7F_j$ (j = 0–4) transitions as a corollary of the direct excitation of Eu^{3+} [50,51]. The strongest peak observed at 614 nm is most likely a result of the forced ED transition ($^5D_0 \rightarrow {}^7F_2$), and the intensity ratio of the $^5D_0 \rightarrow {}^7F_2$ to $^5D_0 \rightarrow {}^7F_1$ transition is substantially large. This ratio is a common indicator of the symmetry of the environment around the doped Ln^{3+} ions [52]. The large ratio obtained from the emission spectrum confirms that the Eu^{3+} ions were located in the low symmetry site. Therefore, it was determined that the 4f-4f transition could be allowed. For the excitation spectrum (Fig. 9a), the observed peaks at 396, 416, 466, and 534 nm can be converted to 3.13, 2.98, 2.66, and 2.32 eV, respectively, using the following equation:

$$E\ (eV) \approx 1240/\lambda\ (nm),$$

where E is the energy and λ is the wavelength. These energy levels are approximately in accordance with the energy states of $^5L_6$, $^5D_3$, $^5D_2$, and $^5D_1$ respectively [50,51], and are assigned to the typical 4f-4f transitions of Eu^{3+} ions. In addition to these results, a broad PL feature in the range of approximately 450–550 nm was observed (data not shown). This feature is likely a result of oxygen defects in the Y_2O_3 crystals [11]. Surface defects such as oxygen defects, often cause a decrease in the emission intensities. However, for the surface defects located near the conduction band, much higher energy states than the ^5D_j states of Eu^{3+} ions are present in the band gap of Y_2O_3 [51]. Therefore, the surface defects may not play a significant role with respect to nonradiative relaxation among the lower ^5D_j states. Another possible cause for the decreasing emission intensity may be phonon resonance originating from some form of crystal defects or lattice distortions, as mentioned in the previous section.

Desirable PL features are recognized by the peak position, whereas a wide full width at

half maximum of each excitation and emission peak indicates an insufficient crystallinity and low homogeneity of the Eu^{3+} distribution over the Y_2O_3 host. We plan to continue to carry out various experiments to improve the PL efficiency from this aspect.

3. Mechanical properties of PMMA adhesives containing the Y_2O_3:Eu^{3+} particles

The yielding stress of the 2% specimen decreased significantly when compared to the 0% and 4% specimens. It is likely that dispersion strengthening as a result of a stress transfer mechanism does not occur. However, the degree of deterioration in the strength is quite definite. An improvement in the dispersion and surface wettability of the particles by certain methods such as a silane treatment may contribute to the reinforcement of the PMMA adhesives. In that case, the increase in the total surface area as a result of the decrease of the particle size would also contribute to reinforcement.

Conclusion

We attempted to dope lattices of Y_2O_3 with trivalent Eu^{3+} ions in order to produce orthodontic adhesives that would be visible upon irradiation with near-ultraviolet light. The crystals synthesized in this study exhibited a submicron size and a very narrow size distribution. The results of the XRD and the EDS analyses led to the conclusion that Y_2O_3:Eu^{3+} particles were adequately synthesized using the homogeneous precipitation method. The spectra of the PMMA adhesives containing Y_2O_3:Eu^{3+} particles exhibited characteristic excitation and emission peaks corresponding to the 4f-4f transitions of Eu^{3+}, despite the PL intensity being relatively low. The yielding loads of the PMMA specimens containing Y_2O_3:Eu^{3+} particles did not deteriorate by a significant amount. Based on the results obtained in this study, we concluded that it is feasible to add Eu^{3+}-doped Y_2O_3 crystalline particles to orthodontic adhesives.

References

1) Campbell PM. Enamel surfaces after orthodontic bracket debonding. Angle Orthod 1995; 65: 103– 110.
2) Radlanski RJ. A new carbide finishing bur for bracket debonding. J orofac Orthop 2001; 62: 296–304.
3) Hosein I, Sherriff M, Ireland AJ. Enamel loss during bonding, debonding, and cleanup with use of a self-etching primer. Am J Orthod Dentofacial Orthop 2004; 126: 717–724.
4) Eliades T, Gioka C, Eliades G, Makou M. Enamel surface roughness following debonding using two resin grinding methods. Eur J Orthod 2004; 26: 333–338.
5) Bonetti GA, Zanarini M, Parenti SI, Lattuca M, Marchionni S, Gatto MR. Evaluation of enamel surfaces after bracket debonding: An in-vivo study with scanning electron microscopy. Am J Orthod Dentofacial Orthop 2011; 140: 696–702.
6) Uo M, Okamoto M, Watari F, Tani K, Morita M, Shintani A. Rare earth oxide-containing fluorescent glass filler for composite resin. Dent Mater J 2005; 24: 49–52.
7) Eliseeva SV, Bünzli JC. Lanthanide luminescence for functional materials and bio-sciences. Chem Soc Rev 2010; 39: 189–227.
8) Yamagata S, Hamba Y, Nakanishi K, Abe S, Akasaka T, Ushijima N, Uo M, Iida J, Watari F. Introduction of rare-earth-element-contaoning ZnO nanoparticles into orthodontic adhesives. Nano Biomedicine 2012; 4: 11–17.
9) Yamagata S, Iwasaki H, Hamba Y, Nakanishi K, Ushijima N, Abe S, Akasaka T, Watari F, Iida J. An evaluation of fluorescent orthodontic adhesives containing Eu-doped ZnO at room temperature. Nano Biomedicine 2013; 5: 31–38.
10) Andelman T, Gordonov S, Busto G, Moghe PV, Riman RE. Synthesis and cytotoxicity of Y_2O_3 nanoparticles of various morphologies. Nanoscale Res Lett 2010; 5: 263–273.
11) Dai Q, Foley ME, Breshike CJ, Lita A, Strouse GF. Ligand-passivated Eu:Y_2O_3 nanocrystals as a phosphor for white light emitting diodes. J Am Chem Soc 2011; 133; 15475–15486.
12) Devaraju MK, Yin S, Sato T. Eu^{3+}:Y_2O_3 microspheres and microcubes: A supercritical synthesis and characterization. Inorg Chem 2011; 50: 4698–4704.
13) de Moura AP, de Oliveira LH, Paris EC, Li MS, Andrés J, Varela JA, Longo E, Rosa IL. Photolumiscent properties of nanorods and nanoplates Y_2O_3:Eu^{3+}. J Fluoresc 2011; 21: 1431–1438.

14) Atabaev TS, Kim HK, Hwang YH, Submicron Y_2O_3 particles codoped with Eu and Tb ions: Size controlled synthesis and tuning the luminescence emission. J Colloid Interface Sci 2012; 373: 14–19.

15) Sharma PK, Jilavi MH, Nass R, Schmidt H. Tailoring the particle size from μm □ nm scale by using a surface modifier and their size effect on the fluorescence properties of europium doped yttria. J Luminescence 1999; 82: 187–193.

16) Goldburt ET, Kulkarni B, Bhargava RN, Taylor J, Libera M. Size dependent efficiency in Tb doped Y_2O_3 nanocrystalline phosphor. J Luminescence 1997; 72–74: 190–192.

17) Vecht A, Gibbons C, Davies D, Jing X, Marsh P, Ireland T, Silver J, Newport A, Barber D. Engineering phosphors for field emission displays. J Vac Sci Technol B 1999; 17: 750–757.

18) Zhou YH, Lin J, Yu M, Han SM, Wang SB, Zhang HJ. Morphyology control and luminescence properties of YAG:Eu phosphors prepared by spray pyrolysis. Mater Res Bull 2003; 38: 1289–1299.

19) Zaki MI, El-Ammawy HA, Baird T. Texture assessment of ceria by analysis of nitrogen sorption isotherms and high-resolution electron microscopy. J Colloid Interface Sci 1988; 126: 450–462.

20) minagawa Y, Yajima F. New preparative method of fine powder of yttrium (III) oxide by thermal decomposition of $NH_4Y(C_2O_4)_2 \bullet H_2O$ fine crystal obtained by reaction of a strongly acidic solution of yttrium oxalate and an aqueous ammonia solution. Bull Chem Soc Jpn 1990; 63: 378–382.

21) Ransijn CDS, Winnubst AJA, Kerkwijk B, Burggraaf AJ, Verweij H. Production of defect-poor nanostructured ceramics of yttria-zirconia. J Eur Ceram Soc 1997; 17: 831–841.

22) Durán P, Villegas M, Fernández JF, Capel F, Moure C. Theoretically dense and nanostructured ceramics by pressureless sintering of nanosized Y-TZP powders. Mater Sci Eng A 1997; 232: 168–176.

23) Garg A, Matijević E. Preparation and properties of uniform coated inorganic colloidal particles: III. Zirconium hydrous oxide on hematite. J Colloid Interface Sci 1988; 126:243–250.

24) Keklikian LD, Matijević E. Needle-type colloidal copper (II) hydroxide particles. Colloid Polym Sci 1990; 268: 1151–1158.

25) Aiken B, Hsu WP, Matijević E. Preparation and properties of uniform mixed and coated colloidal paticles. J Mater Sci 1990; 25: 1886–1894.

26) Jing X, Ireland T, Gibbons C, Barber DJ, Silver J, Vecht A, Fern G, Trowga P, Morton DC. Control of Y_2O_3:Eu^{3+} spherical particle phosphor size, assembly properties, and performance for FED and HDTV. J Electrochem Soc 1999; 146: 4654–4658.

27) He Y, Tian Y, Zhu Y. Large-scale synthesis of luminescent Y_2O_3:Eu nanobelts. Chem Lett 2003; 32: 862–863.

28) Sohn S, Kwon Y, Kim Y, Kim D. Synthesis and characterization of near-monodisperse yttria particles by homogeneous precipitation method. Powder Technology 2004; 142: 136–153.

29) Yoo HS, Jang HS, Im WB, Kang JH, Jeon DY. Particle size control of a monodisperse spherical Y_2O_3:Eu^{3+} phosphor and its photoluminescence properties. J Master Res 2007; 22: 2017–2024.

30) Ozaki M, Kratohvil S, Matijević E. Formation of monodispersed spindle-type hematite particles. J Colloid Interface Sci 1984; 102: 146–151.

31) Gherardi P, Matijević E. Interactions of precipitated hematite with preformed colloidal titania dispersions. J Colloid Interface Sci 1986; 109: 57–68.

32) Hsu WP, Rönnquist L, Matijević E. Preparation and properties of monodispersed colloidal particles of lanthanide compounds: 2. Cerium (IV). Langmuir 1988; 4: 31–37.

33) Sharma PK, Jilavi MH, Naβ R, Schmidt H. Seeding effect in hydrothermal synthesis of nanosize yttria. J Mater Sci Lett 1998; 17: 823–825.

34) Jiang YD, Wang ZL, Zhang F, Paris HG, Summers CJ. Synthesis and characterization of Y_2O_3:Eu^{3+} powder phosphor by a hydrolysis technique. J Mater Res 1998; 13: 2950–2955.

35) Jin T, Jin E, Sano M, Chi B, Yazawa T. Fabrication and luminescent characteristics of Y_2O_3:Eu^{3+} nanotubes by hydrothermal treatment. Chem Lett 2008; 37: 370–371.

36) Hench LL, West JK. The sol-gel process. Chem Rev 1990; 90: 33–72.

37) Dhanaraj J, Jagannathan R, Kutty TRN, Lu CH. Photoluminescence characteristics of Y_2O_3:Eu^{3+} nanophosphors prepared using sol-gel thermolysis. J Phys Chem B 2001; 105: 11098–11105.

38) Wu GS, Lin Y, Yuan XY, Xie T, Cheng BC, Zhang LD. A novel synthesis route to Y_2O_3:Eu nanotubes. Nanotechnology 2004; 15: 568–571.

39) Chong MK, Pita K, Kam CH. Photoluminescence of Y_2O_3:Eu^{3+} thin film phosphors by sol-gel deposition and rapid thermal annealing. J Phys Chem Solids 2005; 66: 213–217.

40) Devaraju MK, Yin S, Sato T. Solvothermal synthesis and characterization of blue, green and red emitting Y_2O_3:Ln^{3+} (Ln^{3+} = Tm^{3+}, Tb^{3+} and Eu^{3+}) nanocrystals. IOP Conf. Series: Mater Sci Eng 2009; 1: 012011 doi: 10.1088/1757-8981/1/1/012011.

41) Devaraju MK, Yin S, Sato T. Synthesis and characterization Y_2O_3:Eu^{3+} nanocrystals prepared via solvothermal refluxing route. Mater Sci Eng C 2009; 29: 1849–1854.

42) Lee MH, Oh SG, Yi SC. Preparation of Eu-doped Y_2O_3 luminescent nanoparticles in nonionic reverse microemulsions. J Colloid Interface Sci 2000; 226: 65–70.

43) Zhang WW, Xu M, Zhang WP, Yin M, Qi ZM, Xia SD, Claudine G. Site-selective spectra and time-resolved spectra of nanocrystalline Y_2O_3:Eu. Chem Phys Lett 2003; 376: 318–323.

44) Chavan SV, Pillai KT, Tyagi AK. Combustion synthesis of nanocryrstalline yttria: Tailoring of powder properties. Mater Sci Eng B 2006; 132: 266–271.

45) Jung KY, Han KH. Densification and photoluminescence improvement of Y_2O_3 phosphor particles prepared by spray pyrolysis. Electrochem Solid-State Lett 2005; 8: H17–H20.

46) Joffin N, Dexpert-Ghys J, Verelst M, Baret G, Garcia A. The influence of microstructure on luminescent properties of Y_2O_3:Eu prepared by spray pyrolysis. J Lumin 2005; 113: 249–257.

47) Hirai T, Hirano T, Komasawa I. Preparation of Y_2O_3:Eu^{3+} phosphor fine particles using an emulsion liquid membrane system. J Mater Chem 2000; 10 2306–2310.

48) Giesche H, Matijević E. Preparation, characterization, and sinterability of well-defined silica/yttria powders. J Mater Res 1994; 9: 436–450.

49) Zhang WW, Zhang WP, Xie PB, Yin M, Chen HT, Jing L, Zhang YS, Lou LR, Xia SD. Optical properties of nanocrystalline Y_2O_3:Eu^{3+} depending on its odd structure. J Colloid Interface Sci 2003; 262: 588–593.

50) Gupta BK, Haranath D, Saini S, Singh VN, Shanker V. Synthesis and characterization of ultra-fine Y_2O_3:Eu^{3+} nanophosphors for luminescent security ink applications. Nanotechnology 2010; 21: 055607 doi: 10.1088/0957-4484/21/5/055607.

51) Bai X, Song H, Yu L, Yang L, Liu Z, Pan G, Lu S, Ren X, Lei Y, Fan L. Luminescent properties of pure cubic phase Y_2O_3/Eu^{3+} nanotubes/nanowires prepared by a hydrothermal method. J Phys Chem B 2005; 109: 15236–15242.

52) Pandey A, Roy MK, Pandey A, Zanella M, Sperling RA, Parak WJ, Samaddar AB, Verma HC. Chloroform- and water-soluble sol-gel derived Eu^{+++}/Y_2O_3 (red) and Tb^{+++}/Y_2O_3 (green) nanophosphors: Synthesis, characterization, and surface modification. IEEE Trans Nanobioscience 2009; 8: 43–50.

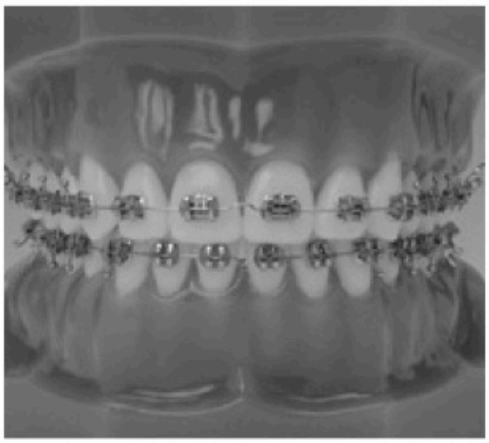

Figure 1 Image of a multibracket appliance.

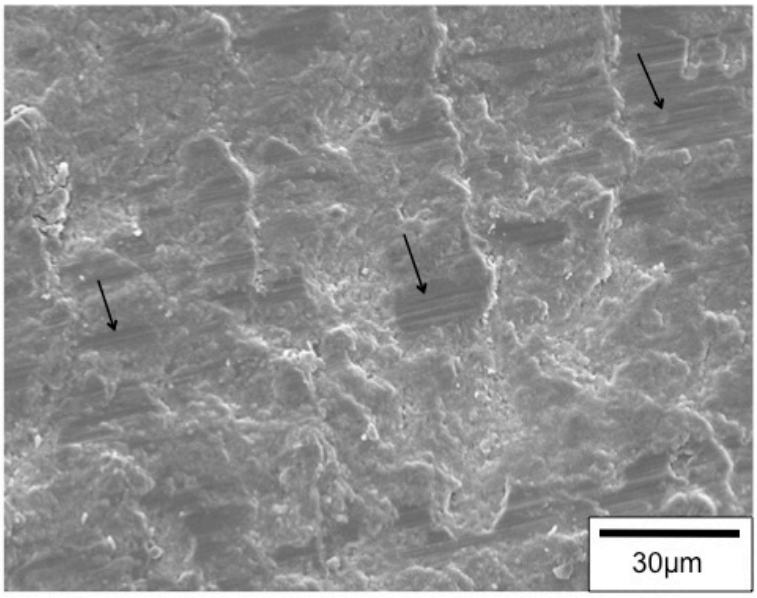

Figure 2 SEM image of an enamel surface after the removal of orthodontic adhesives. An example of typical damage on the enamel surface by a rotary dental instrument is indicated by the arrows.

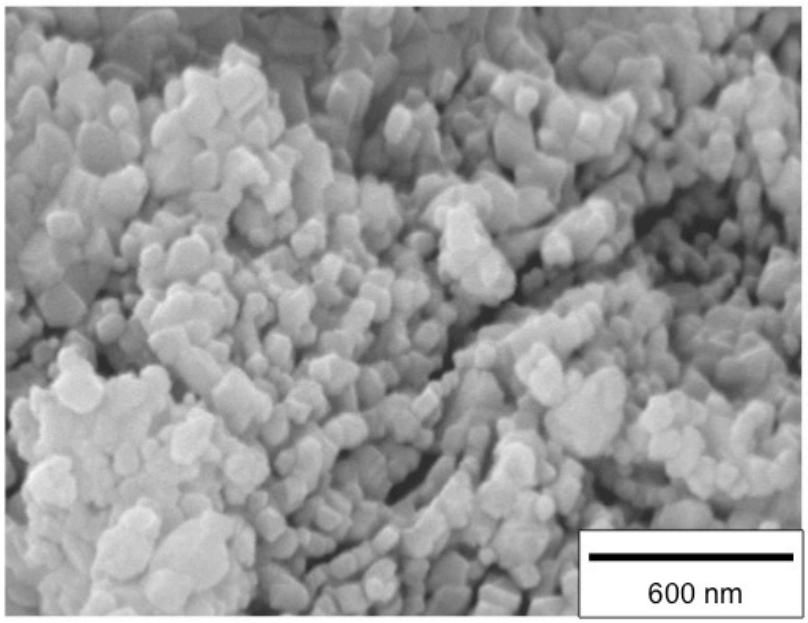

Figure 3 SEM image of the Y_2O_3:Eu^{3+} particles.

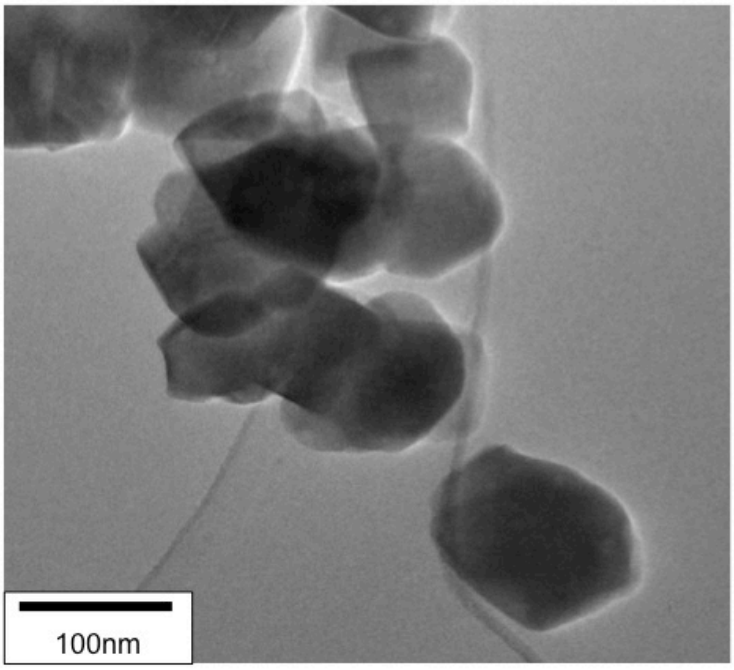

Figure 4 TEM image of the Y_2O_3:Eu^{3+} particles.

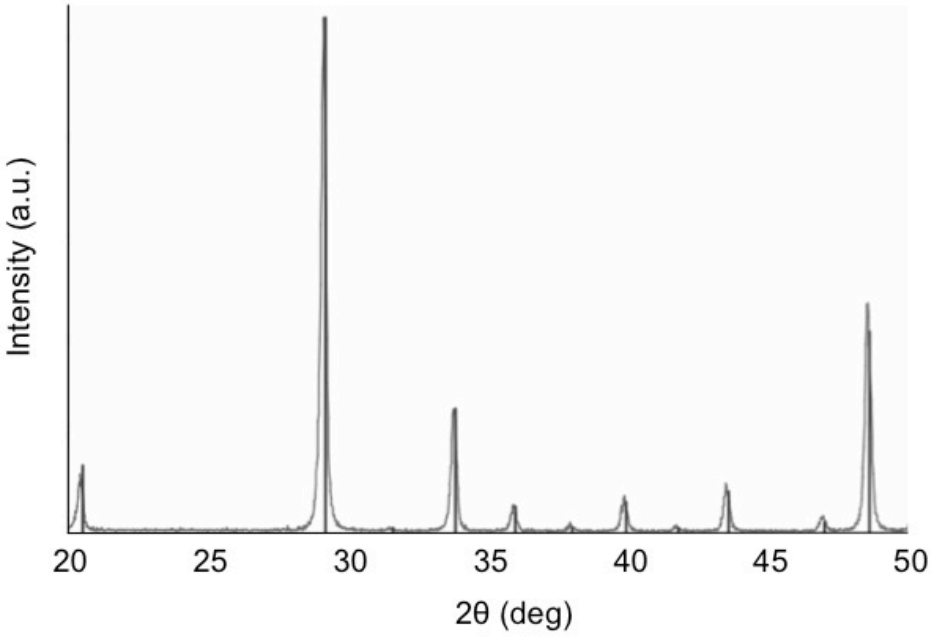

Figure 5 XRD pattern of the Y_2O_3:Eu^{3+} particles.

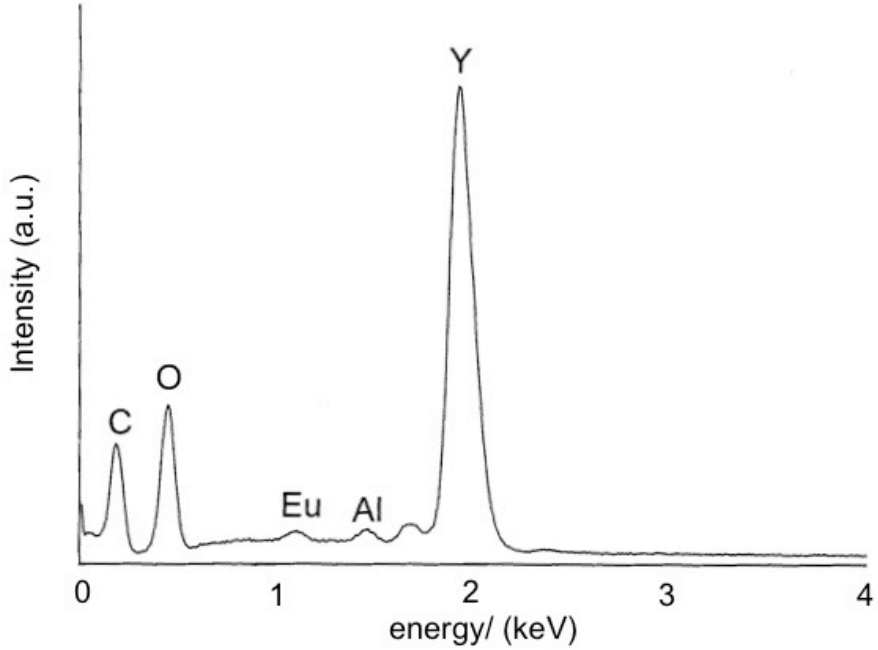

Figure 6 EDS spectrum of the Y_2O_3:Eu^{3+} particles.

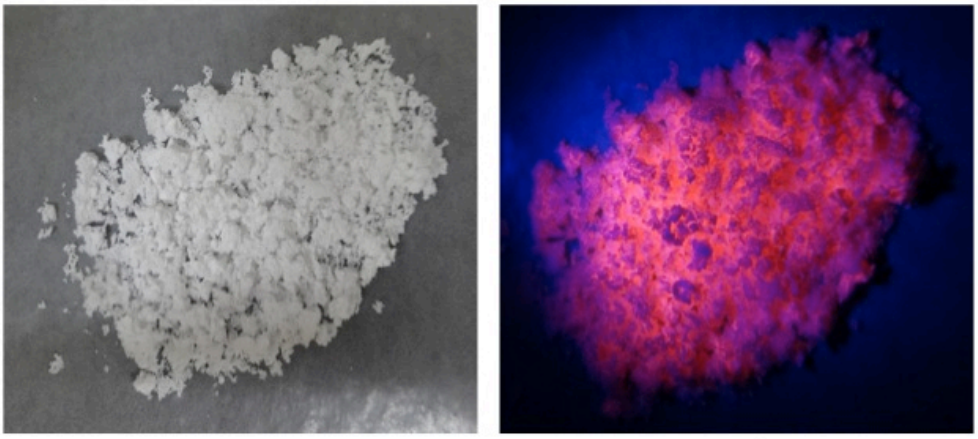

a b

Figure 7 $Y_2O_3:Eu^{3+}$ particles and their fluorescence
a) under natural light and b) under irradiation of near-ultraviolet light .

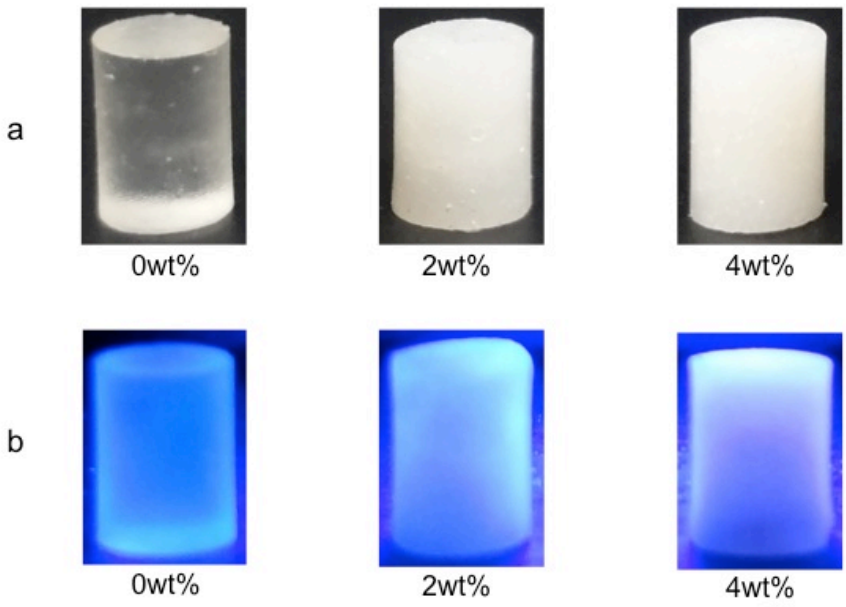

Fig.8 PMMA specimens containing varying amounts of particles and their fluorescence a) under natural light and b) under irradiation of near-ultraviolet light.

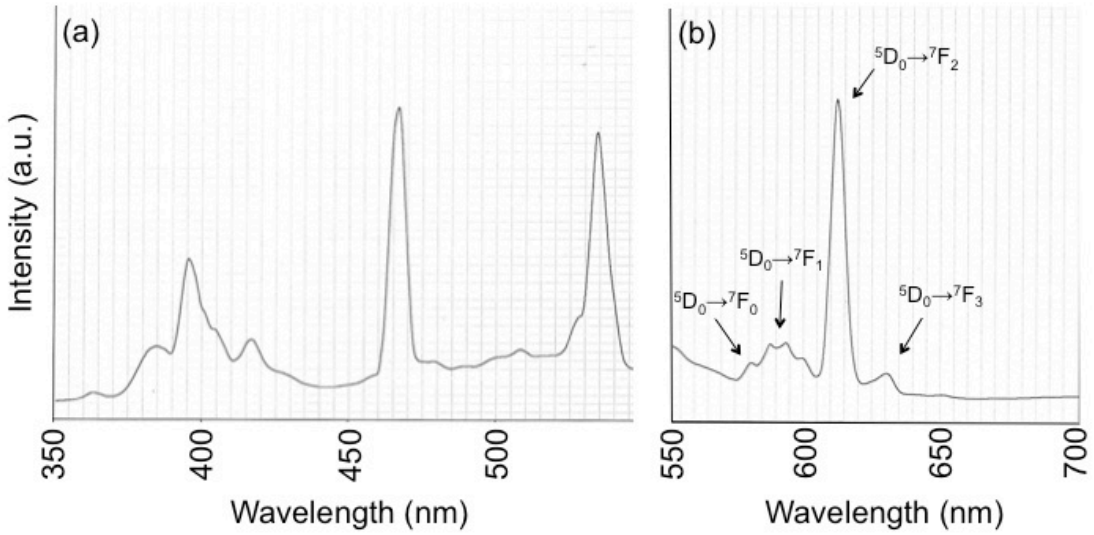

Fig.9 Excitation and emission spectra of the PMMA adhesives containing Y_2O_3:Eu^{3+} particles

a) when the emission at 614 nm was monitored and b) under irradiation at 396 nm.

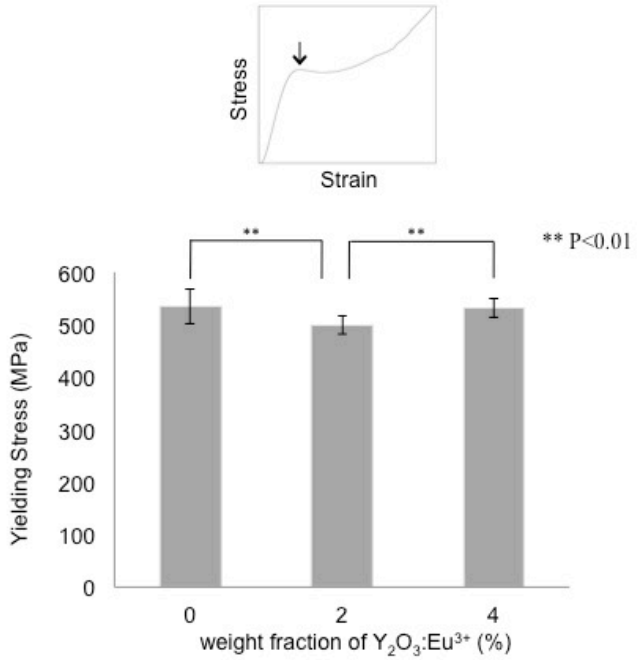

Figure 10 The results of the compression tests.
The inserted figure is an exemplary stress-strain curve of a PMMA specimen. The yielding point is indicated by the arrow.